Bioorganic Chemistry 92 (2019) 103259

Contents lists available at ScienceDirect

Bioorganic Chemistry

journal homepage: www.elsevier.com/locate/bioorg

Tyrosinase inhibitory effects of *Vinca major* and its secondary metabolites: Enzyme kinetics and *in silico* inhibition model of the metabolites validated by pharmacophore modelling

Suat Sari[a], Burak Barut[b], Arzu Özel[b,c], Didem Şöhretoğlu[d,*]

[a] Hacettepe University, Faculty of Pharmacy, Department of Pharmaceutical Chemistry, Sıhhiye, Ankara, TR-06100 Ankara, Turkey
[b] Karadeniz Technical University, Faculty of Pharmacy, Department of Biochemistry, Trabzon, Turkey
[c] Karadeniz Technical University, Drug and Pharmaceutical Technology Application and Research Center, Trabzon, Turkey
[d] Hacettepe University, Faculty of Pharmacy, Department of Pharmacognosy, Sıhhiye, Ankara, Turkey

ARTICLE INFO

Keywords:
Vinca
Iridoid
Tyrosinase
Molecular modelling

ABSTRACT

In the present study, we aimed to identify the tyrosinase enzyme inhibitory potential of *Vinca major* L. extract and its secondary metabolites. The extract possessed remarkable tyrosinase enzyme inhibitory effect with IC_{50} value of 20.39 ± 0.44 μg/mL compared to the positive control, kojic acid (IC_{50} 8.56 ± 0.17 μg/mL). Compounds **1** and **5** were the most potent isolates with IC_{50} values of 32.41 ± 0.99 and 31.34 ± 0.75 μM, they were more potent than kojic acid (IC_{50}: 60.25 ± 0.54 μM). Compound **2** also exhibited remarkable tyrosinase inhibition with an IC_{50} value of 64.51 ± 1.29 μM. An enzyme kinetics analysis revealed that **1** was a mixed-type, **2** and **5** were noncompetitive inhibitors. Using molecular docking, we predicted binding affinity and interactions of the compounds, which were in good alignment with a pharmacophore hypothesis generated out of a number of known tyrosinase inhibitors. The modelling studies underlined crucial interactions with the copper ions and residues around them such as Asn260, His263, and Met280.

1. Introduction

Tyrosinase (EC 1.14.18.1), known as polyphenol oxidase enzyme, is widely distributed in plant, fungi, animals, and bacteria. It catalyzes the hydroxylation of L-tyrosine to 3,4-dihydroxy-L-phenylalanine (L-DOPA) and oxidation of L-DOPA to dopaquinone by using molecular oxygen [1,2]. Then, dopaquinone generates biopigments such as melanin, which protects the skin from UV damage by several reactions. The excessive production of melanin causes freckles, melanoma, and age spots [3]. Also, this pigment has been observed in the brain and it is associated with neurodegenerative disorders like Parkinson and related neurodegenerative disorders [4,5]. Moreover, tyrosinase is one of the main problems of browning fruits and vegetables, leading to quicker degradation and deterioration of nutritional values [6]. The use of tyrosinase inhibitors has attracted great attention in the cosmetic and pharmaceutical industries due to their preventive effects in pigmentation disorders. Thus, finding new tyrosinase inhibitors with lower side effects is desirable.

Genus *Vinca* is used for circulatory disorders, hypertension, diabetes, cerebral circulatory impairment, and as support for brain metabolism [7]. There are five *Vinca* species (Apocynaceae) growing in Turkey [8]. *V. major* is an evergreen shrub with ornamental and medicinal properties. Due to diverse structures and biological effects, alkaloids of *V. major* have been the subject of intense research. However, research on the non-alkaloid constitutes of this plant is very limited [9,10]. Previously, we isolated a phenolic acid, chlorogenic acid (**1**), five iridoids ((7a)-7-O-methylmorroniside (**2**), loganic acid (**3**), vinmajoroside (**4**), 7-*O*-*p*-coumaroylloganin (**5**), loganin (**7**)) and a monoterpenoid glucoindole alkaloid (5 (S)-5-carboxyvincoside) (**6**) from the leaves of *V. major* [9]. In the present study, we tested tyrosinase inhibitory effects of *V. major* extract as well as the isolated compounds (**1**–**7**) (see Fig. 1).

The availability of target crystal structures makes structure-based modelling of enzyme inhibition easier, which can be supported by ligand-based approaches such as QSAR, similarity search, molecular finger prints, and pharmacophore modelling. In order to provide insights in to inhibition mechanisms of the title compounds, we performed molecular docking studies in the catalytic site of tyrosinase. We evaluated how good the binding modes of these compounds aligned with the pharmacophore model we generated using the known inhibitors of tyrosinase.

* Corresponding author.
E-mail address: didems@hacettepe.edu.tr (D. Şöhretoğlu).

https://doi.org/10.1016/j.bioorg.2019.103259
Received 29 May 2019; Received in revised form 9 July 2019; Accepted 4 September 2019
Available online 05 September 2019
0045-2068/

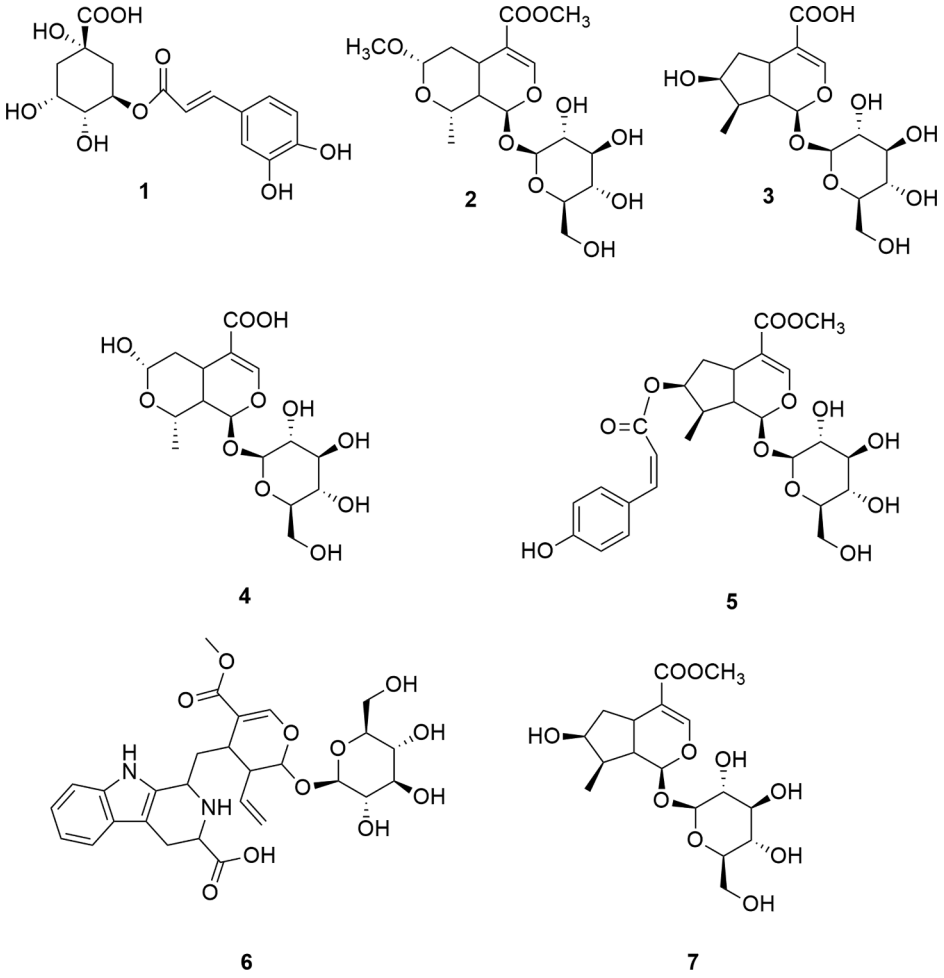

Fig. 1. Structures of **1–7**.

Table 1
IC_{50} values of the isolated compounds against tyrosinase.

Compounds	IC_{50} (μM)
1	32.41 ± 0.99[#]
2	64.51 ± 1.29
3	126.42 ± 4.33
4	107.86 ± 2.75
5	31.34 ± 0.75[#]
6	94.73 ± 1.56
7	117.32 ± 3.52
Kojic Acid	60.25 ± 0.54

[#] $p < 0.001$ compared to kojic acid.

2. Materials and methods

2.1. Materials and reagents

V. major leaves L. were collected from Yeditepe University Campus, Kayisdagi, Istanbul, Turkey by Prof. Dr. Hasan Kirmizibekmez. A voucher specimen has been deposited in the Herbarium of Department of Pharmacognosy, Faculty of Pharmacy, Yeditepe University, Istanbul, Turkey (YEF 10016)). The tested compounds were isolated as previously described [9]. L-DOPA, kojic acid, tyrosinase from mushroom, and methanol were obtained from Sigma-Aldrich (St. Louis, MO). Tyrosinase inhibitory effects of the samples were determined using Multiskan™ Go Microplate Spectrophotometer with a 96-well microplate reader.

2.2. Mushroom tyrosinase inhibition assay

The mushroom tyrosinase (Sigma, T3824) inhibition of methanol extract and isolated compounds was carried out by following our previously reported methods [11]. Kojic acid (Sigma, K3125) was used as a positive control. First, 100 μL of 100 mM phosphate buffer (pH 6.8), 20 μL of 250 U/mL mushroom tyrosinase and 20 μL inhibitor solution was prepared in 96 well plates. After pre-incubation for 10 min at room temperature, the reaction was initiated with 20 μL of 3 mM L-DOPA (Sigma, D9628) addition into the plates which were incubated for 10 min at room temperature. Then, optical density (OD) was determined at 475 nm using a microplate reader (Thermo Scientific Multiskan). The fifty percent inhibitory concentration (IC_{50}) was determined using the formula; % inhibition: (A-B)/A × 100, where A is the activity of the enzyme without inhibitor and B is the activity of the enzyme with inhibitor.

2.3. Mushroom tyrosinase inhibition kinetic analysis

In order to investigate the inhibitory types and constants of compound **1**, **2**, and **5** against mushroom tyrosinase, Lineweaver-Burk and Dixon plots were used [12,13]. The experiments were performed using the same protocol described above with several concentrations of L-DOPA (2.5, 5, 7.5, and 10 mM) or inhibitors (20, 30, and 40 μM for compound **1** and **5**; 40, 60, and 80 μM for compound **2**). Graphs were generated using Microsoft Excel Windows 10.

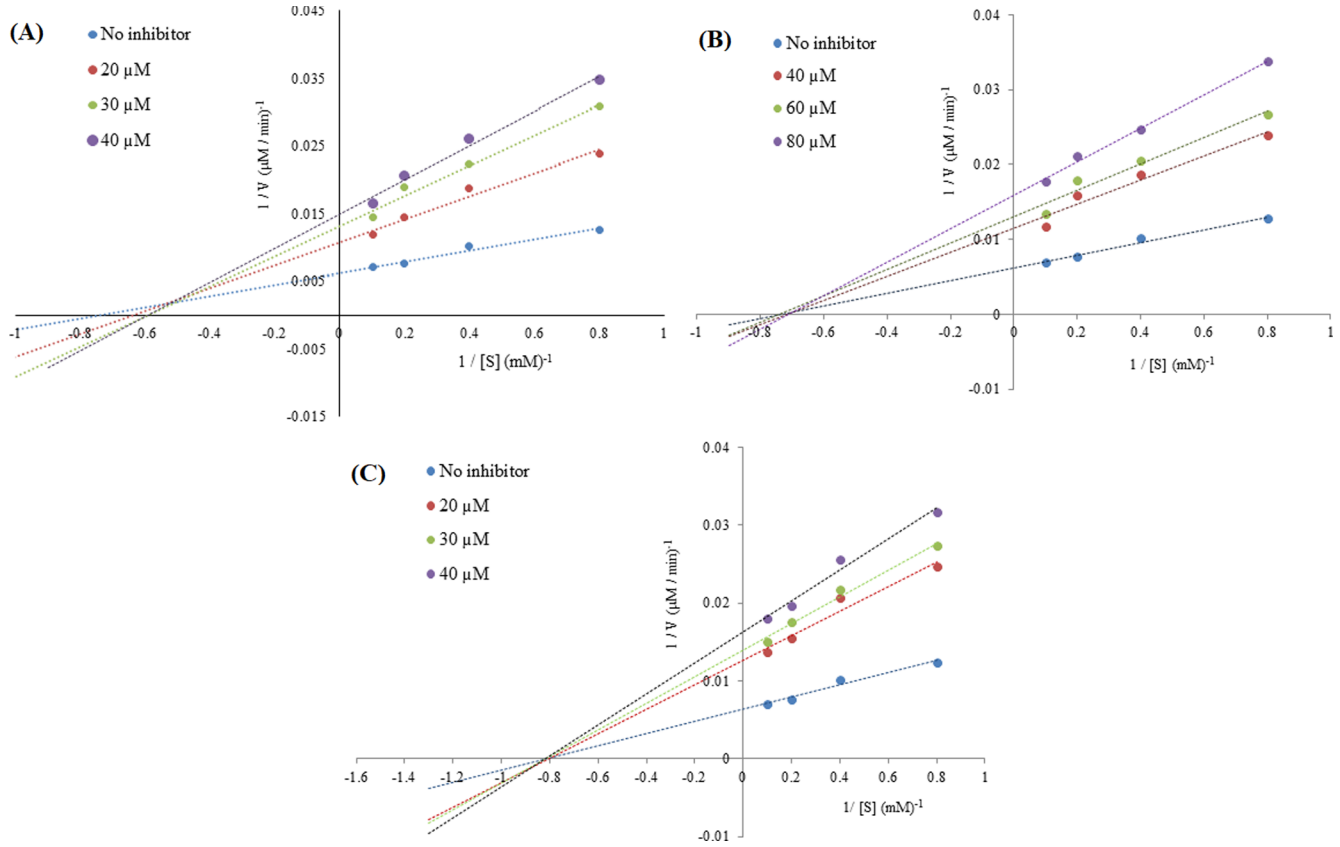

Fig. 2. Lineweaver-Burk plots for the inhibition of tyrosinase in the presence of **1** (**A**), **2** (**B**) and **5** (**C**).

Table 2
K_i values and inhibition types of compound 1, 2, and 5 against tyrosinase.

Compounds	Type	K_i
1	Mixed	15.30 ± 0.26
2	Non-competitive	43.20 ± 0.25
5	Non-competitive	29.50 ± 0.32
Kojic Acid	Competitive	–

2.4. Statistical analysis

Data were analyzed using Microsoft Excel Windows 10 and GraphPad Prism 5.0. The results were expressed as mean ± standard deviation (n = 3). The differences among the compounds were investigated by one-way analysis of variance (ANOVA) followed by Tukey tests. $p < 0.001$ was considered to be significant.

2.5. Molecular modeling

Ligand models were generated using MacroModel (2018-4: Schrödinger, LLC, NY, 2018) and OPLS_2005 force field parameters, and optimized using conjugate gradient method [14]. Their molecular descriptors and pharmacokinetic properties were calculated using QikProp (2018-4: Schrödinger, LLC, NY, 2018). The crystal structure of tyrosinase from *Agaricus bisporus* (mushroom) co-crystallized with tropolone (PDB ID: 2Y9X, resolution: 2.78 Å [15]) was downloaded from RCSB Protein Data Bank (PDB) (www.rcsb.org) [16] and prepared using Protein Preparation Wizard of Maestro (2018–4: Schrödinger, LLC, NY, 2018) [17] by assigning bond orders, hydrogen atoms and OPLS charges, generating ionization and tautomeric states with Epik (2018-4: Schrödinger, LLC, New York, NY, 2018), and setting proton positions with Propka. Receptor grids of 20 $Å^3$ were prepared using grid generation module of Maestro by taking the central coordinates of tropolone (-0.62 26.99-43.78). Molecular docking was performed using Glide (2018-4: Schrödinger, LLC, New York, NY, 2018) at extra precision (XP) mode with 50 runs for each ligand [18–20]. Binding poses were visually inspected on Maestro and the XP GScore of the best pose for each ligand was noted. To test the accuracy of XP Glide, we re-docked the co-crystallized ligand, tropolone, to the active site of the enzyme using the settings above and the RMSD value of the docking conformer regarding the co-crystalized conformer was found 1.33 Å.

The compounds used for building pharmacophore hypotheses were modelled and minimized as described for the title compounds. A number of hypotheses were generated using Phase (2018-4: Schrödinger, LLC, New York, NY, 2018) [21,22] by aligning a maximum of 50 conformers for each compound, limiting the number of features 3 to 5, and setting the feature tolerance to 2 Å. The PhaseHypoScore and BEDROC score for each hypothesis were noted. Then, the title compounds were screened against all the pharmacophore hypotheses created. The binding conformer of each compound obtained from docking was used in the screening instead of generating new conformers. The PhaseScreenScore was used to evaluate their fitness to each hypothesis.

3. Results and discussion

3.1. Inhibitory properties of the extract and the isolated compounds on mushroom tyrosinase

The IC_{50} values of methanol extract and isolated compounds against tyrosinase were determined according to the protocol described above. The results were summarized in Table 1 and Fig. 2.

The IC_{50} value of methanol extract was found to be 20.39 ± 0.44 µg/mL. All the isolated compounds inhibited tyrosinase with IC_{50} values ranging from 31.34 ± 0.75 to 126.42 ± 4.33 µM. Compounds **1** and **5** displayed the most potent inhibition against

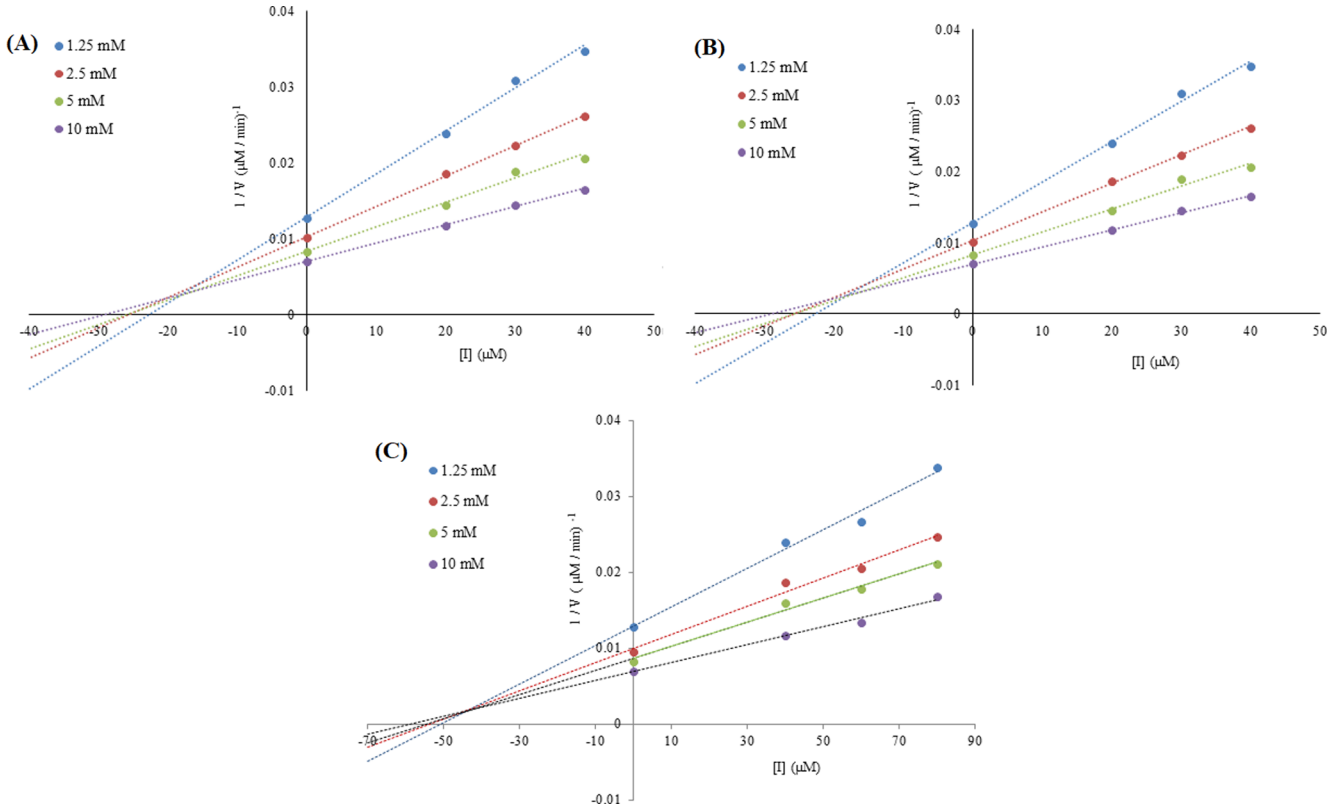

Fig. 3. Dixon plots for the inhibition of tyrosinase in the presence of **1** (**A**), **2** (**B**) and **5** (**C**).

Table 3
Calculated molecular descriptors of the title compounds and their ideal values ranges.

	MW	RB	HD	HA	LogP	PSA (Å^2)	LogS
Comp.	(130.0–725.0)	(0–15)	(0.0–6.0)	(2.0–20.0)	(-2.0–6.5)	(7.0–200.0)	(-6.5–0.5)
1	354.3	10	6	9.7	−0.3	186.6	−2.6
2	420.4	9	4	17.3	−1.5	158.8	−2.3
3	376.4	9	6	15.6	−1.8	178.5	−2.0
4	392.4	9	6	17.3	**−2.3**	187.3	−1.9
5	536.5	13	5	16.7	0.1	201.4	−4.5
6	574.6	12	**7**	17.4	−1.9	**206.8**	−3.3
7	390.4	9	5	15.6	−1.6	164.2	−2.4

*Values outlying the ideal ranges are highlighted as **bold**.

Table 4
Docking scores of the compounds (kcal/mol).

1	**2**	**3**	**4**	**5**	**6**	**7**
−9.81	−6.18	−5.85	−6.17	−7.48	−5.92	−5.50

tyrosinase with IC_{50} values of 32.41 ± 0.99 and 31.34 ± 0.75 µM, respectively. Both compounds possessed higher tyrosinase inhibitory effect than kojic acid (IC_{50}: 60.25 ± 0.54 µM) used as a positive control. The rest of the compounds showed lesser effect compared to kojic acid. According to the literature, the phenolic compounds display very strong tyrosinase inhibitory effects due to the hydroxyl groups possibly by forming hydrogen bonds with the enzyme catalytic site [23]. The only differences between the structure of **5** and **7** are that **5** is 7-*O*-coumaroyl substituted derivative of **7**. The IC_{50} value of compound **5** was about 3.75 times lower than that of compound **7**. This finding suggests that the presence of the coumaroyl group enhanced tyrosinase inhibition.

3.2. Kinetic mechanism of mushroom tyrosinase inhibition

In this study, we selected the most potent inhibitors (compounds **1**, **2**, and **5**) of mushroom tyrosinase for kinetic analysis on the basis of IC_{50} values. Lineweaver-Burk and Dixon analyzes of the compounds were shown in Table 2, Figs. 2 and 3.

Lineweaver-Burk plots (plot of 1/V vs 1/[S]) were obtained at different concentrations of the compounds and substrate to determine the type of inhibition. As shown in Fig. 2, the results of Lineweaver-Burk plots for compounds **2** and **5** showed that K_m remained the same, while V_{max} decreased with increasing concentrations. This behavior indicated that compound **2** and **5** were non-competitive inhibitors of tyrosinase. On the other hand, compound **1** inhibited tyrosinase in a mixed manner since K_m and V_{max} went up with increasing concentrations. Dixon plots (plot of 1/V vs [I]) of the slope toward the concentration of inhibitor showed K_i values. It is known that the lower the Ki value the tighter the binding with the enzyme, which makes the inhibitor more effective. The K_i values of compounds **1**, **2**, and **5** were found as 15.30 ± 0.26, 43.20 ± 0.25, and 29.50 ± 0.32 µM, respectively.

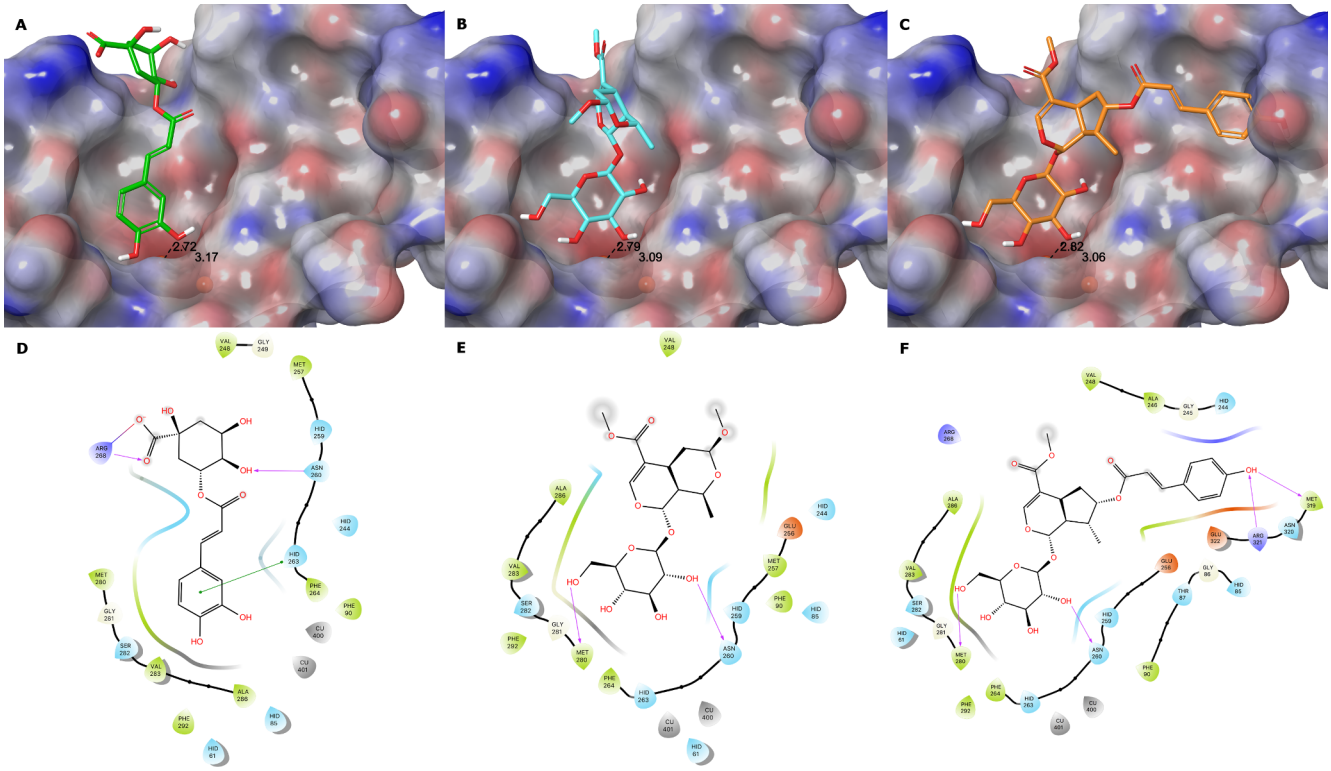

Fig. 4. Binding modes of compounds **1** (A), **2** (B), **5** (C), and their binding interactions in 2D diagrams (D-F, respectively). In A-C, the ligands are represented as color sticks, the copper ions as orange spheres, and the molecular surface of the binding site residues are rendered in color according to the electrostatic potential of the atoms; distances (in Å) between the copper ions and the coordinating oxygens are labelled. In D-F, the binding interactions are represented as color lines/arrows (H bond: magenta, π-π: green, salt bridge: blue/red).

3.3. Molecular modelling of mushroom tyrosinase inhibition

3.3.1. Evaluation of the drug-like chemical space

Qikprop calculates a number of pharmaceutically relevant molecular descriptors and pharmacokinetic properties, and provides values ranges for comparing a particular molecule's properties with those of 95% of known drugs. Among these descriptors; molecular weight (MW), number of rotatable bonds (RB), H bond donor and acceptor counts (HD and HA), logarithmic coefficient of octanol/water partition (LogP), and polar surface area (PSA) are used to define the drug-like chemical space [24–26]. Aqueous solubility (LogS) is also considered a challenging pharmacokinetic issue in drug discovery [27]. We calculated these molecular descriptors for the title compounds and compared the results with the ideal values ranges provided by QikProp (Table 3).

According to the calculated values, the compounds mostly fall into the drug-like chemical space except a few exceptions. **6**'s H bond donor count and polar surface area values fall out of the ideal range, and **4**'s calculated LogP is too low. Good aqueous solubility was calculated for the title compounds, as well. These findings indicate that the title compounds may represent drug candidates in terms of their pharmacokinetic profile.

3.3.2. Molecular docking to mushroom tyrosinase

Tyrosinase catalytic site is located at the heart of two antiparallel α helix pairs including two Cu^{2+} ions, hence the name binuclear copper-binding site. Each copper ion coordinates with water and three histidine residues: His61, His85, His94, and His259, His263, His296 [15,28]. His85 is linked to Cys83 side chain with a thioether bond, both of which are also connected by a threonine residue. The motif formed by these residues are conserved among mushroom tyrosinases [29]. The copper-coordinating histidines also contact with nearby residues, limiting their side chain flexibility and stabilizing the catalytic site for substrates. It is, therefore, important to interact with these binding side residues and copper ligands beside the copper ions themselves for the inhibitors to be effective [15,30].

Upon molecular docking, compound **1** showed the highest affinity to the tyrosinase active site (Table 4). The scores of other compounds also indicate good affinity to the site compared to Kojic acid's previously reported docking score (−4.80 kcal/mol). In **1**'s binding mode, the caffeoyl group perfectly sits to the catalytic gorge stabilized through a π-π interaction with His263 side chain, which puts the hydroxyl oxygen at the third position of the benzene ring within the interaction distance to the copper ions (Fig. 4). The length of the propenoyl linker between the 3,4-dihidroxyphenyl and the sugar moieties also allows the latter to interact with the polar entry and narrow neck residues effectively (see salt bridge and H bond interactions with Asn260 and Arg268 in Fig. 4) and lets the polar groups at the sugar moiety be disposed to water. The propenoyl linker ideally fits in the narrow neck between the entry and the catalytic gorge. In the case of **2** and **5**, the catalytic gorge is occupied by their sugar moieties, which are stabilized through H bonds with Asn260 and Met280. The hydroxyl at the 4th position of the sugar of both derivatives engages with the coppers. An extra cavity in the catalytic gorge is occupied by the *p*-coumaroyl of **5** and this moiety makes H bonds with Met319 and Arg321, and van der Waals contacts with Glu322 in this cavity, which probably explains the potency of this inhibitor as suggested above (Fig. 4). The importance of this extra cavity was highlighted in our previous studies, as well [31,32]. **2**, however, lacks interactions with both the entry and the extra cavity residues, also the hydrophobic methyl groups of **2** facing the entry are somewhat solvent exposed, which is not desired. The residues mentioned above were reported to line the active site of mushroom tyrosinase and similar interactions and binding modes were found in several *in silico* studies [11,31–34].

3.3.3. Validation of the docking results by pharmacophore modelling

There are numerous reports in the literature featuring molecular

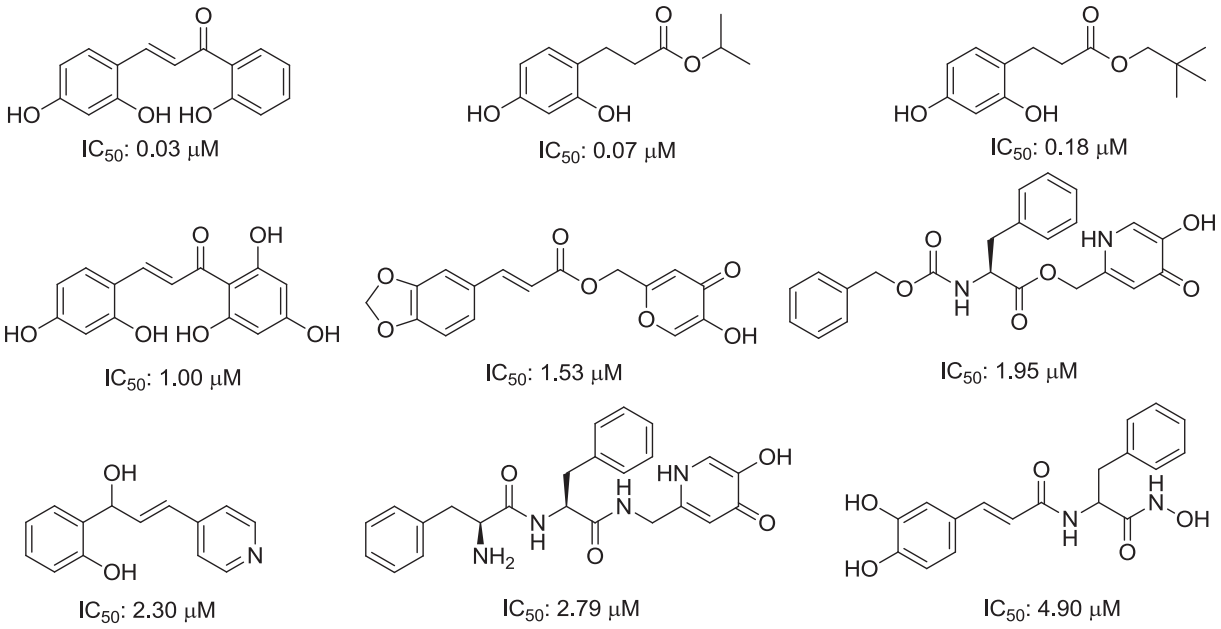

Fig. 5. The mushroom tyrosinase inhibitors selected from the literature to create the pharmacophore hypothesis.

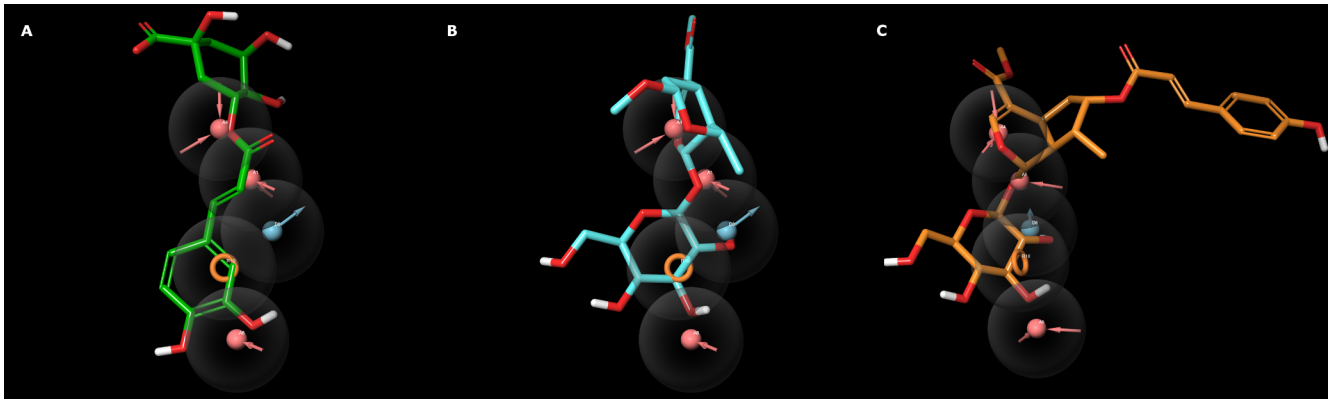

Fig. 6. Alignment of compound **1** (A), **2** (B), and **5** (C) with the pharmacophore hypothesis. The H bond acceptor features are represented as red, H bond donor feature as blue spheres, and the ring feature as orange ring. The direction of H bond donation are showed as color arrows and the tolerance spaces as transparent spheres. The ligands are represented as color sticks.

docking with mushroom tyrosinase, however pharmacophore modelling studies are rare [35–38]. For the first time in this study, we tried to validate the docking results of the most active derivatives by pharmacophore modelling. For this purpose, we randomly selected nine mushroom tyrosinase inhibitors with IC_{50} values ranging between 0.01 and 5 μM (Fig. 5) [39–45].

The pharmacophore hypothesis (PhaseHypoScore: 0.79, BEDROC Score: 60) created out of these inhibitors consisted of five features: three H bond acceptor groups, one H bond donor group and one ring, which spatially aligned close to each other to form a zigzag. The docking poses of compounds **1**, **2**, and **5** (PhaseScreenScore: 1.39, 0.96, and 0.93, respectively), showed good alignment with this hypothesis (Fig. 6). The oxygen atoms of these compounds that coordinate with the copper ions align with the first acceptor feature of the hypothesis, supporting the oxygen-Cu^{2+} interaction observed in the docking studies. The ring feature positioned close to this acceptor feature aligns well with the rings of the compounds facing the copper ions, too. The donor feature of the hypothesis matches with the hydroxyl groups of **2** and **5**, which donate H bond to Asn260 backbone oxygen. **1**, however, fails to fulfill this pharmacophore. Another acceptor group aligns with the carbonyl oxygen of the propenoyl of **1**, the oxygen linking the pyranopyran and the sugar of **2**, and the oxygen between the cyclopentapyran and sugar moieties of **5** (Fig. 6). These oxygens were found in electrostatic contact with Asn260 side chain NH in the docking studies (Fig. 4). These findings, in general, support the accuracy of the molecular docking results.

4. Conclusions

In this study, we tested tyrosinase potential of *V. major* and secondary metabolites isolated from this plant. Especially, among the isolated compounds, **1** and **5** were stronger tyrosinase inhibitors than the positive control, kojic acid. Compound **1** was a mixed-type, whereas **2** and **5** were non-competitive inhibitors of tyrosinase.

Docking poses and interactions of compounds **1**, **2**, and **5** in tyrosinase active site feature close interactions with the copper ions, as well as some of the key residues in this site, such as His263, Asn260, Arg268, and Met280, which were supported by the excellent alignment of these poses with our pharmacophore hypothesis. The ability of compound **5** to effectively occupy the extra cavity in the active site with its *p*-coumaroyl moiety was considered one of the key aspects of this compound's inhibitory potential.

Appendix A. Supplementary material

Supplementary data to this article can be found online at https://doi.org/10.1016/j.bioorg.2019.103259.

References

[1] A. Sánchez-Ferrer, J.N. Rodríguez-López, F. García-Cánovas, F. García-Carmona, Tyrosinase: a comprehensive review of its mechanism, Biochim. Biophys. Acta 1247 (1995) 1–11.

[2] H. Decker, F. Tuczek, Tyrosinase/catecholoxidase activity of hemocyanins: structural basis and molecular mechanism, Trends Biochem. Sci. 25 (2000) 392–397.

[3] F. Solano, Melanins: skin pigments and much more—types, structural models, biological functions, and formation routes, Article number 498276, New J. Sci. (2014), https://doi.org/10.1155/2014/498276.

[4] I. Carballo-Carbajal, A. Laguna, J. Romero-Giménez, T. Cuadros, J. Bové, M. Martinez-Vicente, A. Parent, et al., Brain tyrosinase overexpression implicates age-dependent neuromelanin production in Parkinson's disease pathogenesis, Nat. Commun. 10 (2019) Article number 973.

[5] M. Asanuma, I. Miyazaki, N. Ogawa, Dopamine- or L-DOPA-induced neurotoxicity: the role of dopamine quinone formation and tyrosinase in a model of Parkinson's disease, Neurotox. Res. 5 (2003) 165–176.

[6] S. Parvez, M. Kang, H.S. Chung, H. Bae, Naturally occurring tyrosinase inhibitors: mechanism and applications in skin health, cosmetics and agriculture industries, Phytother. Res. 21 (2007) 805–816.

[7] T. Fleming, PDR for Herbal Medicines, 3rd ed., Medical Economics Co., Montvale, NJ, 2004, pp. 632–633.

[8] M. Koyuncu, G. Ekşi, A.M. Gençler Özkan, *Vinca ispartensis* (Apocynaceae), a New Species from Turkey, Ann. Bot. Fenn. 52 (2015) 340–344.

[9] D. Şöhretoğlu, M. Masullo, S. Piacente, H. Kirmizibekmez, Iridoids, monoterpenoid glucoindole alkaloids and flavonoids from *Vinca major*, Biochem. Syst. Ecol. 49 (2013) 69–72.

[10] G.G. Cheng, H.Y. Zhao, L. Liu, Y.L. Zhao, C.W. Song, J. Gu, W.B. Sun, Y.P. Liu, X.D. Luo, Non-alkaloid constituents of *Vinca major*, Chin. J. Nat. Med. 14 (2016) 56–60.

[11] D. Şöhretoğlu, S. Sari, B. Barut, A. Özel, Tyrosinase inhibition by a rare neolignan: inhibition kinetics and mechanistic insights through *in vitro* and *in silico* studies, Comput. Biol. Chem. 76 (2018) 61–66.

[12] H. Lineweaver, D. Burk, The determination of enzyme dissociation constants, J. Am. Soc. 56 (1934) 658–666.

[13] P. Butterworth, The use of Dixon plots to study enzyme inhibition, Biochim. Biophys. Acta (BBA) – Enzymol. 289 (1972) 251–253.

[14] L. Banks, H.S. Beard, Y. Cao, A.E. Cho, W. Damm, R. Farid, A.K. Felts, T.A. Halgren, D.T. Mainz, J.R. Maple, Integrated modeling program, applied chemical theory (IMPACT), J. Comput. Chem. 26 (2005) 1752–1780.

[15] W.T. Ismaya, H.J. Rozeboom, A. Weijn, J.J. Mes, F. Fusetti, H.J. Wichers, B.W. Dijkstra, B.W. Crystal, Structure of Agaricus bisporus mushroom tyrosinase: identity of the tetramer subunits and interaction with tropolone, Biochemistry 50 (2011) 5477.

[16] H.M. Berman, J. Westbrook, Z. Feng, G. Gilliland, T.N. Bhat, H. Weissig, I.N. Shindyalov, P.E. Bourne, The protein data bank, Nucleic Acids Res. 28 (2000) 235–242.

[17] G.M. Sastry, M. Adzhigirey, T. Day, R. Annabhimoju, W. Sherman, Protein and ligand preparation: parameters, protocols, and influence on virtual screening enrichments, J. Comput. Aid. Mol. Des. 27 (2013) 221–234.

[18] R.A. Friesner, J.L. Banks, R.B. Murphy, T.A. Halgren, J.J. Klicic, D.T. Mainz, M.P. Repasky, E.H. Knoll, D.E. Shaw, M. Shelley, J.K. Perry, P. Francis, P.S. Shenkin, Glide: a new approach for rapid, accurate docking and scoring. 1. Method and assessment of docking accuracy, J. Med. Chem. 47 (2004) 1739–1749.

[19] R.A. Friesner, R.B. Murphy, M.P. Repasky, L.L. Frye, J.R. Greenwood, T.A. Halgren, P.C. Sanschagrin, D.T. Mainz, Extra precision glide: docking and scoring incorporating a model of hydrophobic enclosure for protein-ligand complexes, J. Med. Chem. 49 (2006) 6177–6196.

[20] T.A. Halgren, R.B. Murphy, R.A. Friesner, H.S. Beard, L.L. Frye, W.T. Pollard, J.L. Banks, Glide: a new approach for rapid, accurate docking and scoring. 2. Enrichment factors in database screening, J. Med. Chem. 47 (2004) 1750–1759.

[21] S.L. Dixon, A.M. Smondyrev, E.H. Knoll, S.N. Rao, D.E. Shaw, R.A. Friesner, PHASE: A new engine for pharmacophore perception, 3D QSAR model development, and 3D database screening. 1. Methodology and preliminary results, J. Comput. Aided Mol. Des. 20 (2006) 647–671.

[22] S.L. Dixon, A.M. Smondyrev, S.N. Rao, PHASE: A novel approach to pharmacophore modeling and 3D database searching, Chem. Biol. Drug Des. 67 (2006) 370–372.

[23] T.-S. Chang, An updated review of tyrosinase inhibitors, Int. J. Mol. Sci. 10 (2009) 2440–2475.

[24] C.A. Lipinski, F. Lombardo, B.W. Dominy, P.J. Feeney, Experimental and computational approaches to estimate solubility and permeability in drug discovery and development settings, Adv. Drug Deliv. Rev. 46 (2001) 3–26.

[25] D.F. Veber, S.R. Johnson, H.Y. Cheng, B.R. Smith, K.W. Ward, K.D. Kopple, Molecular properties that influence the oral bioavailability of drug candidates, J. Med. Chem. 45 (2002) 2615–2623.

[26] J.J. Lu, K.K. Crimin, J.T. Goodwin, P. Crivori, C. Orrenius, L. Xing, P.J. Tandler, T.J. Vidmar, B.M. Amore, A.G. Wilson, P.F. Stouten, P.S. Burton, Influence of molecular flexibility and polar surface area metrics on oral bioavailability in the rat, J. Med. Chem. 47 (2004) 6104–6107.

[27] C.F. Stratton, D.J. Newman, D.S. Tan, Cheminformatic comparison of approved drugs from natural product versus synthetic origins, Bioorg. Med. Chem Lett. 25 (2015) 4802–4807.

[28] W.H. Flurkey, J.K. Inlow, Proteolytic processing of polyphenol oxidase from plants and fungi, J. Inorg. Biochem. 102 (2008) 2160–2170.

[29] T. Klabunde, C. Eicken, J.C. Sacchettini, B. Krebs, Crystal structure of a plant catechol oxidase containing a dicopper center, Nat. Struct. Biol. 5 (1998) 1084–1090.

[30] B. Hazes, K.A. Magnus, C. Bonaventura, J. Bonaventura, Z. Dauter, K.H. Kalk, W.G.J. Hol, Crystal structure of deoxygenated Limulus polyphemus subunit II haemocyanin at 2.18 Å resolution: clues for a mechanism for allosteric regulation, Protein Sci. 2 (1993) 597–619.

[31] D. Şöhretoğlu, D.S. Sari, S.B. Barut, A. Özel, Tyrosinase inhibition by some flavonoids: Inhibitory activity, mechanism by *in vitro* and *in silico* studies, Bioorg. Chem. 81 (2018) 168–174.

[32] S. Sari, B. Barut, A. Özel, A.A. Kuruüzüm-Uz, D. Şöhretoğlu, Tyrosinase and α-glucosidase inhibitory potential of compounds isolated from *Quercus coccifera* bark: *In vitro* and *in silico* perspectives, Bioorg. Chem. 86 (2019) 296–304.

[33] Y.L. Xue, T. Miyakawa, Y. Hayashi, K. Okamoto, F.Y. Hu, N. Mitani, M. Tanokura, Isolation and tyrosinase inhibitory effects of polyphenols from the leaves of persimmon *Diospyros kaki*, J. Agric. Food Chem. 59 (2011) 6011–6017.

[34] X. Tan, C. Y-Hun Song, K.-W. Lee Park, J.Y. Kim, D.W. Kim, K.D. Kim, K.W. Lee, M.J. Curtis-Long, K.H. Park, Highly potent tyrosinase inhibitor, neorauflavane from *Campylotropis hirtella* and inhibitory mechanism with molecular Docking, Bioorg. Med. Chem. 24 (2016) 153–159.

[35] N.W. Hsiao, T.S. Tseng, Y.C. Lee, W.C. Chen, H.H. Lin, Y.R. Chen, Y.T. Wang, H.J. Hsu, K.C. Tsai, Serendipitous discovery of short peptides from natural products as tyrosinase inhibitors, J. Chem. Inf. Model. 54 (2014) 3099–3111.

[36] K. Bagherzadeh, F. Talari, A. Sharifi, M.R. Ganjali, A.A. Saboury, M. Amanlou, A new insight into mushroom tyrosinase inhibitors: docking, pharmacophore-based virtual screening, and molecular modeling studies, J. Biomol. Struct. Dyn. 33 (2015) 487–501.

[37] H. Morita, T. Kayashita, K. Takeya, H. Itokawa, Conformational analysis of a tyrosinase inhibitory cyclic pentapeptide, pseudostellarin A, from *Pseudostellaria heterophylla*, Tetrahedron 50 (1994) 12599–12608.

[38] H. Gao, Predicting tyrosinase inhibition by 3D QSAR pharmacophore models and designing potential tyrosinase inhibitors from Traditional Chinese medicine database, Phytomedicine 38 (2018) 145–157.

[39] Z.P. Zheng, Y.N. Zhang, S. Zhang, J. Chen, One-pot green synthesis of 1,3,5-triarylpentane-1,5-dione and triarylmethane derivatives as a new class of tyrosinase inhibitors, Bioorg. Med. Chem. Lett. 26 (2016) 795–798.

[40] S. Khatib, O. Nerya, R. Musa, S. Tamir, T. Peter, J. Vaya, Enhanced substituted resorcinol hydrophobicity augments tyrosinase inhibition potency, J. Med. Chem. 50 (2007) 2676–2681.

[41] Z. Zhou, J. Zhuo, S. Yan, L. Ma, Design and synthesis of 3,5-diaryl-4,5-dihydro-1H-pyrazoles as new tyrosinase inhibitors, Bioorg. Med. Chem. 21 (2013) 2156–2162.

[42] J.C. Cho, H.S. Rho, H.S. Baek, S.M. Ahn, B.Y. Woo, Y.D. Hong, J.W. Cheon, J.M. Heo, S.S. Shin, Y.H. Park, K.D. Suh, Depigmenting activity of new kojic acid derivative obtained as a side product in the synthesis of cinnamate of kojic acid, Bioorg. Med. Chem. Lett. 22 (2012) 2004–2007.

[43] D.Y. Zhao, M.X. Zhang, X.W. Dong, Y.Z. Hu, X.Y. Dai, X. Wei, R.C. Hider, J.C. Zhang, T. Zhou, Design and synthesis of novel hydroxypyridinone derivatives as potential tyrosinase inhibitors, Bioorg. Med. Chem. Lett. 26 (2016) 3103–3108.

[44] S.K. Radhakrishnan, R.G. Shimmon, C. Conn, A.T. Baker, Azachalcones: a new class of potent polyphenol oxidase inhibitors, Bioorg. Med. Chem. Lett. 25 (2015) 1753–1756.

[45] S.Y. Kwak, J.K. Yang, H.R. Choi, K.C. Park, Y.B. Kim, Y.S. Lee, Synthesis and dual biological effects of hydroxycinnamoyl phenylalanyl/prolyl hydroxamic acid derivatives as tyrosinase inhibitor and antioxidant, Bioorg. Med. Chem. Lett. 23 (2013) 1136–1142.